INSTITUTE OF PHYSICS PUBLISHING PLASMA PHYSICS AND CONTROLLED FUSION

Plasma Phys. Control. Fusion **48** (2006) S17–S29 doi:10.1088/0741-3335/48/4/S02

Mean $E \times B$ flows and GAM-like oscillations in the H-1 heliac

M G Shats, H Xia and M Yokoyama[1]

Plasma Research Laboratory, Research School of Physical Sciences and Engineering, Australian National University, Canberra, ACT 0200, Australia

Received 26 August 2005, in final form 30 January 2006
Published 6 March 2006
Online at stacks.iop.org/PPCF/48/S17

Abstract

Experimental results on the connection between mean $E \times B$ flows and coherent oscillations at the frequency of the geodesic acoustic mode (GAM) in the H-1 heliac are presented. An increase in the mean local radial electric field, E_r, is correlated with the development of several coherent modes. As mean E_r increases, spectral energy, which is mostly contained in coherent modes, grows. This is followed by the onset of the $m = 0$, $n = 0$ finite frequency GAM-like mode. Analysis of the heliac magnetic structure shows that geodesic curvature is considerably stronger in H-1 than in tokamaks. A possible role of geodesic oscillations in the transfer of spectral energy from mean zonal flows into coherent modes leading to the generation of the GAM-like mode is discussed. In the proposed scenario of the L–H transition in H-1 the inverse energy cascade leads to the accumulation of turbulence energy in the mean zonal-flow like structure, until geodesic effects lead to the generation of coherent modes and GAM. The coherent modes' parallel phase velocities are very close to the ion thermal velocity suggesting the possibility of their strong Landau damping. It is suggested that the shear decorrelation mechanism eventually forbids the energy transfer from E_r to these modes which reinforces spectral condensation and leads to L–H transition.

(Some figures in this article are in colour only in the electronic version)

1. Introduction

Turbulence-driven zonal flows in magnetized plasma [1] have been extensively studied in the last decade mostly theoretically and computationally (for a review see [2]). Recently a large body of experimental evidence has been presented [3–9], which confirmed many theoretical predictions and suggested several important roles played by zonal flows in toroidal plasma, particularly in the formation of the transport barriers [7, 10, 11].

[1] National Institute for Fusion Science, Toki 509-5292, Japan.

Two main branches of zonal flows have been identified. Both have zero poloidal and toroidal mode numbers, $m = n = 0$. One of them is a zero-frequency, finite-bandwidth zonal flow, while the other is the finite-frequency mode often referred to as a geodesic acoustic mode, or GAM. The latter originates from the geodesic curvature in toroidal geometry and develops as a result of the coupling between mean zonal flow and the $m = 1$, $n = 0$ pressure (density) perturbation [12]. The reason for the $m = 1$ sideband oscillations in the density is the variation in the magnetic field on the flux surface. The radial electric field causes the $E \times B$ flow in the poloidal direction. Since B is not constant in the poloidal direction, it leads to the density accumulation proportional to $E \times B \cdot \nabla B^2/B^4$ [12].

Since GAMs have a distinct frequency, they should be considerably easier to identify in experiments. A linear theory of GAM predicts oscillations at a frequency, which in a tokamak geometry is determined as [2]

$$\omega_{\mathrm{GAM}} \approx \frac{c_{\mathrm{s}}}{R}\sqrt{2 + q^{-2}} \tag{1}$$

Here c_{s} is the ion acoustic velocity, R is a major radius of a tokamak and q is the safety factor. As explained in [2], if the field line has a finite geodesic curvature, the $E \times B$ motion induces compression and turns into a density perturbation if the frequency is in the range of c_{s}/qR or higher. Here $qR = L_{\parallel}$ is the parallel connection length in a tokamak. In stellarators $L_{\parallel}$ should be significantly shorter due to the inherent B-ripple, such that the GAM frequency should be higher, as will be discussed below.

Finite frequency coherent zonal flow-like structures have been observed for the first time in the H-1 heliac [3]. They have been identified as $m = 0$ potential structures having finite radial wave number. Measurements of poloidal, k_θ, and radial, k_r, wave numbers were performed using Langmuir probes which were carefully aligned on the flux surface (for k_θ measurements) and radially displaced (for k_r measurements) with the aid of the electron beam launched into the H-1 magnetic structure before the plasma discharge. Frequency spectra of the fluctuations in the electrostatic potential in H-1 typically show several coherent features in the frequency range below 20 kHz, including zonal flows, as well as broadband turbulence extending beyond 100 kHz. The spectral energy transfer analysis in H-1 [13, 14] has revealed that the inverse energy cascade via three-wave interactions is responsible for the transfer of spectral energy from the spectral region in the range of (20–40) kHz into the lower frequency (and lower wave number) range. However the nonlinear energy transfer (NET) function did not show any fine structure which would correspond to coherent modes. The question whether the inverse energy cascade is responsible for the generation of coherent modes in H-1 could not be resolved on the basis of NET analysis. On the other hand, the amplitude correlation technique [15] applied to the H-1 fluctuation data [14] indicated that there is a noticeable (0.4 or higher) correlation between the unstable spectral range and all the coherent structures. It was also found that the time lag in the amplitude correlation function (ACF) corresponds to the energy flow direction from the broadband turbulence towards the coherent structures.

It is well-known that the inverse energy cascade in the 2D fluid turbulence may lead to the accumulation of turbulent energy in the largest scale (determined by the system size), such that most of the turbulent energy is transformed into energy of one of the largest vortex [16]. In [17] we compared several features of a process of spectral condensation in 2D fluid turbulence which has been reproduced in a 2D fluid experiment, with some of the characteristics (e.g. the evolution of spectra and generation of strong $E \times B$ flow) of the L–H transitions in the H-1 plasma. This study has revealed several interesting similarities pointing to the universality of the turbulence self-organization in toroidal plasma and in 2D fluids. However some differences are inevitable.

One of the obvious differences between spectral condensation in toroidal plasma and in incompressible fluid turbulence would be geodesic coupling of the mean zonal flow discussed above to the low-frequency density/potential oscillations. Such coupling may lead to the generation of the linearly stable $m = 1$, $n = 0$ density perturbations and $m = 0$ potential oscillations [12]. However this linear theory neglects all non-ideal effects which may be important in real experimental situations.

It has been shown in numerical simulations that the energy of the mean zonal flow can be transferred to coherent modes via the geodesic transfer mechanism which acts as a sink and may prevent the growth of zonal flow [18]. Simulations of the tokamak edge turbulence have shown that the zonal flow energy is depleted by toroidal coupling to the pressure and leads to the generation of a relatively large number of sideband modes [19]. This finding has been supported by observations of zonal flows in the ASDEX Upgrade tokamak [9]. It has been noted that the GAM itself, or the $m = 0$, $n = 0$ mode, may not even be clearly observable in the developed sideband mode regime [9]. These results are of great importance for the physics of zonal flows since they offer a mechanism of the zonal flow dissipation in addition to collisional damping.

In this paper we investigate the possible connection of the mean zonal flow (or, more generally, mean E_r) energy to coherent low-frequency oscillations observed in the H-1 heliac, including a GAM-like $m = 0$ mode [3]. We will show that this mode also has $n = 0$ and its development is correlated with the increase in the NET from the broadband turbulence into the mean zonal flow and the onset of several coherent $n \neq 0$ modes whose development precedes the onset of the GAM-like mode. This will be considered in the context of the turbulence–zonal flow interaction summarized in the flowchart of figure 1. The energy reservoir which drives the unstable spectral region in H-1 is the pressure gradient [14]. The energy is transferred to lower wave numbers (frequencies) via the inverse energy cascade [14] forming a broad spectrum of fluctuations. The spectral energy is accumulated in the spectral condensate, seen as the mean zonal flow [17]. Some part of its energy is damped by collisions while some may be transferred via geodesic effects to coherent modes. Both mean zonal flows and GAM can modulate drift-wave turbulence via shearing as discussed in [20], which may lead to the GAM instability. This dynamic shearing is illustrated in figure 1 using dashed lines. However in our experiments this dynamics appears to be more complex because of the strong coherent coupling between mean zonal flow, unstable spectral range, coherent modes and the GAM-like mode (dashed lines). This coherent interaction will not be discussed in detail here. Another important issue which we will discuss is the Landau damping of coherent modes. This seems to play an important role in our experiments and may in particular affect the hypothetic energy transfer from mean $E \times B$ flow to the GAM-range modes.

The paper is organized as follows. Section 2 describes the H-1 heliac and presents experimental results on the interaction between the unstable spectral range, mean zonal flow and coherent oscillations. Measurements of the poloidal and toroidal mode numbers using probes are also described. In section 3 we discuss the analysis of the H-1 magnetic structure relevant for the geodesic transfer mechanism. In section 4 we summarize observations and discuss the possible scenario of the L–H transitions in the H-1 heliac and the role of the interaction between zonal flow, coherent modes and GAMs in these transitions.

2. Spectra of turbulent fluctuations and generation of coherent modes

The reported results were obtained in the H-1 heliac [21], a helical axis stellarator having a major radius of $R_0 = 1.0$ m and a minor plasma radius of less than 0.2 m. The magnetic field structure of H-1 is characterized by a relatively high rotational transform ($1/q = \iota = 1.1$–1.5

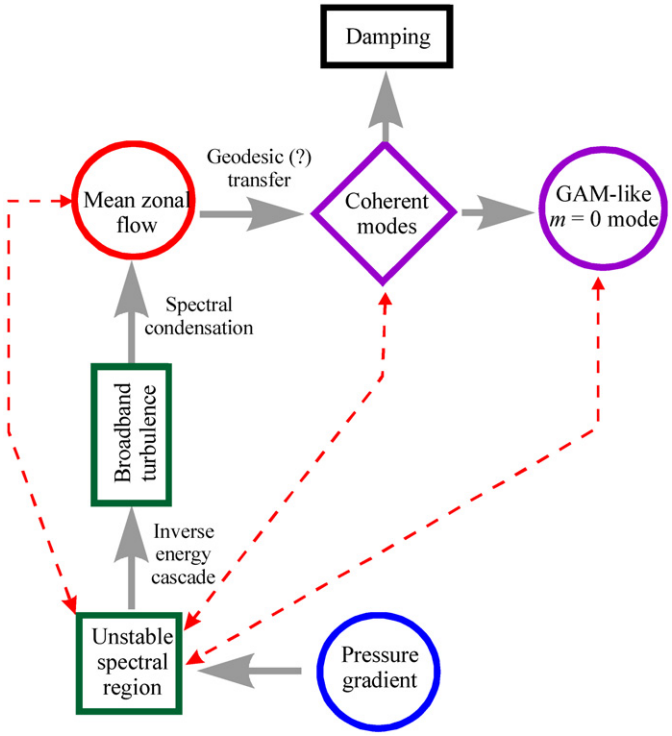

Figure 1. Energy flow in the turbulence zonal flow system.

in the described experiments) and very low magnetic shear ($\hat{s} = (\rho/\iota)(\mathrm{d}\iota/\mathrm{d}\rho) \approx 0.005$–$0.01$). In the experiments discussed here H-1 was operated at low magnetic fields (<0.2 T) with current-free plasma produced by the pulsed radio-frequency (rf) power of less than 100 kW at 7 MHz. The rf power pulse length is about 80 ms. The electron temperature in the discharge is low enough ($T_\mathrm{e} = 5$–30 eV) so that Langmuir probes can be used throughout the plasma cross-section. Here we present results obtained in argon discharges.

As has been discussed in several previous publications from H-1 (e.g. [22,23]) spontaneous L–H transitions coinciding with a strong reduction in turbulence and confinement improvement are observed when the magnetic field reaches some critical value. It has also been shown [23] that the increase in magnetic field coincides with the increase in the ion temperature, T_i, and in the radial electric field, E_r.

Processes leading to the confinement improvement during the B scan can be summarized as follows. When B is increased, ion temperature also increases with B such that the ion pressure gradient goes up [23]. This is followed by the increase in E_r, in agreement with the radial force balance in H-1, where $E_r \approx (Z_\mathrm{i} e n_\mathrm{i})^{-1} \nabla P_\mathrm{i}$, and contributions from the $V_\mathrm{i} \times B$ components to the balance are small. Thus, better ion confinement due to the B increase leads to the build-up of E_r and perhaps, eventually to the suppression of turbulence. It has also been shown that levels of the threshold E_r and its shear agree pretty well with the shear decorrelation criteria for the low poloidal mode number fluctuations which dominate the L-mode spectrum before the transition to H-mode. Below we present a somewhat different point of view (however consistent with the above description) on the processes leading to the transition.

Figure 2 shows a spectrum of fluctuations in the floating potential measured in L-mode at $\rho = 0.5$. The broadband part of the spectrum at $f > 30$ kHz shows a clear power law

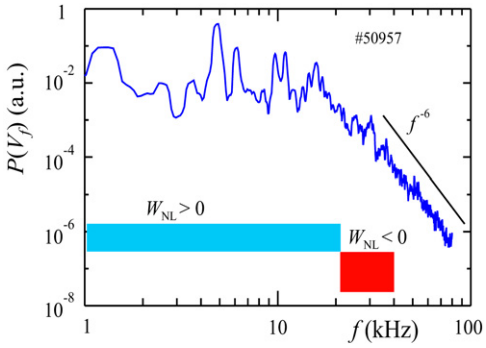

Figure 2. Auto-power spectrum of the floating potential fluctuations in H-1 at $\rho = 0.5$ in L-mode at $B = 0.062$ T.

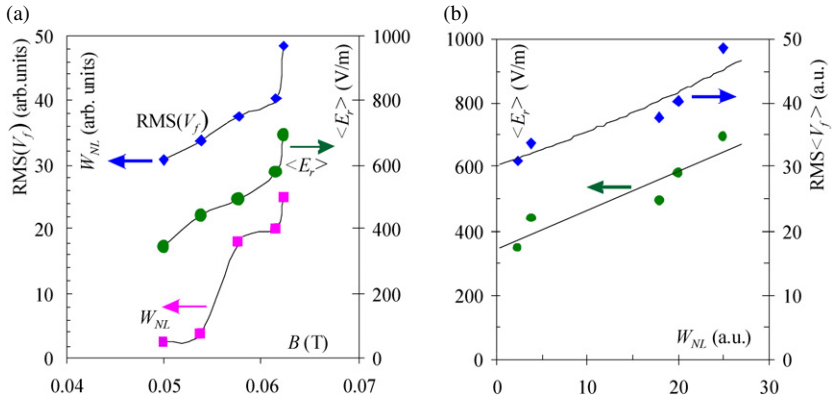

Figure 3. (*a*) The NET from the unstable range, $|W_{\rm NL} < 0|$ (□), mean radial electric field, $\langle E_r \rangle$ (●), and the root-mean-square value of the fluctuation level, RMS($V_{\rm f}$) (◇), versus the magnetic field in L-mode; (*b*) $\langle E_r \rangle$ (●) and RMS($V_{\rm f}$) (◇) versus $|W_{\rm NL} < 0|$ estimated at $\rho = 0.5$.

trend $P \sim f^{-6}$ over more than three decades. As discussed in [13] such scaling is universal for L-mode and is consistent with the theoretically expected energy spectrum of electrostatic turbulence $W \sim k^{-4}$ in the enstrophy cascade range [26], since $W \sim (1 + k^2)P$.

At $f < 20$ kHz several strong coherent modes are seen. These coherent modes contain over 90% of the overall spectral power. The spectral energy transfer analysis of such spectra [14] has shown the NET due to three-wave interactions from the spectral range of $f \approx$ (20–40) kHz into the low-frequency range $f < 20$ kHz. This is illustrated in figure 2 by two shaded boxes corresponding to the regions of negative ($W_{\rm NL} < 0$) and positive ($W_{\rm NL} > 0$) NET function. The spectral region where $W_{\rm NL} < 0$ has been identified as the region of the underlying pressure-gradient-driven instability [14].

During the magnetic field scan, this energy, $|W_{\rm NL} < 0|$, increases with the increase in B, or more precisely, with the increase in the plasma pressure gradient [14]. This increase is shown in figure 3(*a*). Correlated with the increase in $|W_{\rm NL} < 0|$, mean zonal flow ($\langle E_r \rangle$) also increases with B. The root-mean-square level of the potential fluctuations (dominated by coherent modes) also increases with B. By excluding the B-dependence one could present these results as the increase in $\langle E_r \rangle$ and in the level of coherent modes due to the increase in nonlinear energy transferred from the unstable range into mean zonal flow and then into

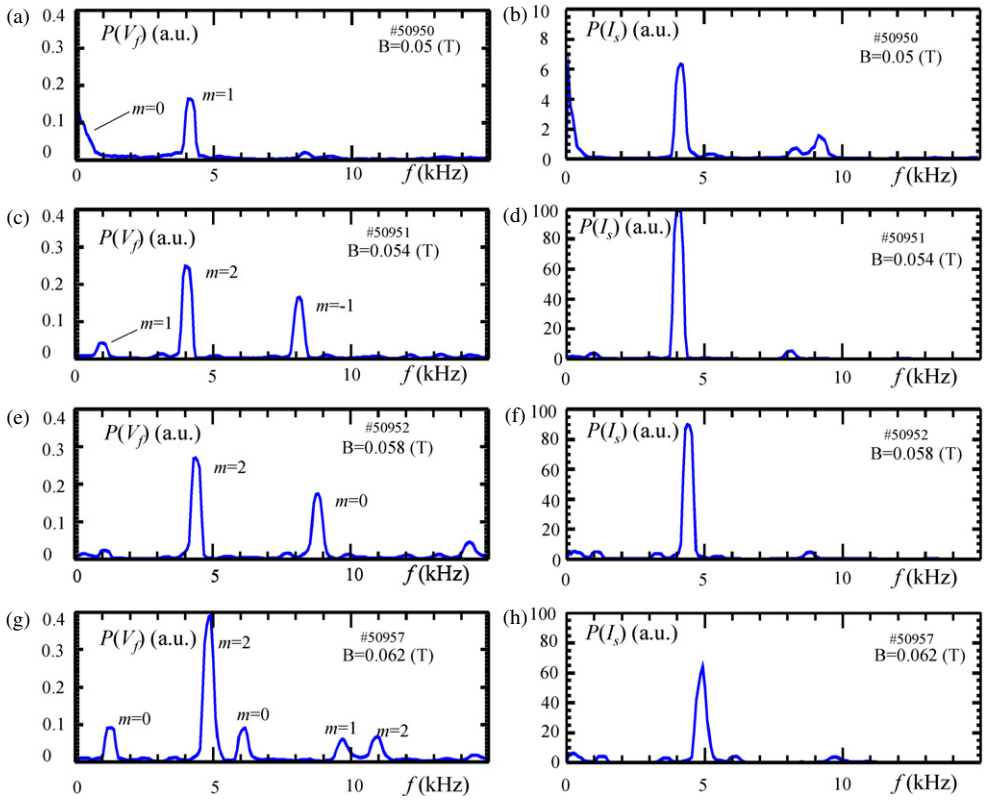

Figure 4. Auto-power spectra of the fluctuations in the floating potential, $P(V_\mathrm{f})$, (left column), and in the ion saturation current ($I_\mathrm{s} \sim n_\mathrm{e}$), $P(I_\mathrm{s})$, (right column), during the magnetic field scan in L-mode.

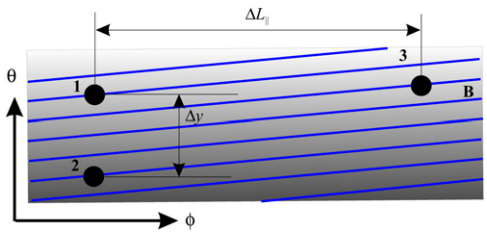

Figure 5. Schematic of the probe arrangement for the determination of the fluctuation wave numbers.

coherent modes. This is illustrated in figure 3(*b*), where both $\langle E_r \rangle$ and $RMS(\tilde{V}_\mathrm{f})$ increase proportionally with $|W_\mathrm{NL} < 0|$.

It is not clear, however, from the above results how coherent modes develop as the magnetic field and $\langle E_r \rangle$ increase. This was studied during the B-scan as illustrated in figure 4 which shows evolution of spectra of the fluctuations in the floating potential and in the ion saturation current ($I_\mathrm{s} \sim n_\mathrm{e}$).

Figure 5 shows a schematic of the probes set-up used for the determination of the poloidal and toroidal wave numbers of the potential fluctuations. Two probe tips (1 and 2) are separated poloidally by $\Delta y = 34$ mm, while the third probe tip (3) was positioned about $\Delta L_\parallel = 0.5$ m

away in the toroidal direction from the first two. Poloidal wave numbers are derived from the phase shift $\Delta\varphi_{12}$ measured using two poloidally separated probes (1 and 2) set to the same flux surface as described above: $m(f) = k_\theta(f)r = r(\Delta\varphi_{12}(f)/\Delta y)$. The 3rd probe is set on the same flux surface as probes 1 and 2 using the electron beam. However aligning it to the same poloidal angle as, for example, probe 1 is rather difficult. Nevertheless, it is possible to estimate toroidal wave number using data from all three probes. A phase shift between signals measured by probes 1 and 3 is determined by its toroidal and poloidal components

$$\Delta\varphi_{13}(f) = k_\parallel(f)\Delta L_\parallel + k_\theta(f)\Delta y_{13}, \tag{2}$$

where $\Delta L_\parallel$ and Δy_{13} is the toroidal and poloidal separation between probes 1 and 3, respectively, and $k_\theta(f)$ is known from the phase between probes 1 and 2. The second term on the right-hand side of equation (2) is zero for the $m = 0$ mode, which makes determination of the toroidal mode number of this mode more reliable due to the independence of the uncertainty in the poloidal separation Δy_{13}. Errors in the determination of Δy_{13} are responsible for errors in the $k_\parallel$ measurements.

During the B-scan fluctuation spectra evolve as shown in figure 4. At the lowest B corresponding to the lowest $\langle E_r \rangle$ (corresponding to the lowest $|W_{\mathrm{NL}} < 0|$) both the V_f and the I_s spectra are dominated by the $f = 4.1$ kHz mode which has poloidal mode number $m = 1$ as seen in figures 4(a) and (b). At $f < 1$ kHz poloidally symmetric structure ($m = 0$) is seen in V_f, which corresponds to the spectrally broadened mean (zero-frequency) zonal flow.

As $\langle E_r \rangle$ (as well as $|W_{\mathrm{NL}} < 0|$ and B) is increased, several other coherent modes having $m = (0, 1, 2, \ldots)$ are observed as seen in figures 4(c)–(h). The $m = 0$ modes are the time varying oscillations in the radial electric field [3] which typically have a frequency between 4 and 9 kHz.

Toroidal mode numbers of the spectral components shown in figure 4(g) have been measured as described above. For the $m = 0$ mode at $f = 6.2$ kHz a parallel wave number of $k_\parallel \approx 0.2\,\mathrm{m}^{-1}$ unambiguously suggests $n = k_\parallel \mathrm{R} \approx 0$. This confirms the similarity of this mode to the GAM. It should be noted, however, that these GAM-like structures are observed together with other $m = (1, 2, \ldots)$ coherent modes and have never been observed in H-1 as solely coherent features in the potential spectra. An increase in B above the level at which these $m = 0, n = 0$ modes are observed often coincides with the transition to H-mode followed by a strong reduction in the fluctuation level of both coherent modes and broadband turbulence. When the magnetic field is close to the threshold, finite-frequency zonal flows play an important role in the dynamics of spontaneous L–H transitions in H-1 as discussed in [11].

The $f = 4.8$ kHz mode in figure 4(g) has $m = 2$ and $k_\parallel = (2.4\text{–}3.4)\,\mathrm{m}^{-1}$ which suggests $n = k_\parallel \mathrm{R} \approx 2$ or 3. Similarly estimated mode numbers for the $f = 4.1$ kHz mode in figure 4(a) are $m = 1$ and $n = 1$ (or 2).

The $m = 1, n = 1(2)$ spectral feature observed in the fluctuations of the floating potential (figure 4(a)) is spectrally coupled to the $m = 0$ low-frequency oscillations at $f \approx 0$. The analysis of this spectral connection is performed in the frequency domain using the amplitude correlation technique [25]. This technique has been successfully used to analyse spectral transfer in H-1 [14, 17]. Two frequency bands of interest, namely, $f_1 = (0.25 \pm 0.2)$ kHz and $f_2 = (4.1 \pm 0.2)$ kHz are selected from the potential fluctuation signal by band-pass-filtering it in order to obtain two time series. These two time series are then squared and passed through a low-pass filter to obtain only the slow varying amplitude information. Then the cross-correlation function between these signals is computed (using a 50 ms time sample split into four 50% overlapping time segments), to obtain the ACF,

$$\mathrm{ACF}(\tau) = \langle [x_1^2(t)][x_2^2(t+\tau)] \rangle. \tag{3}$$

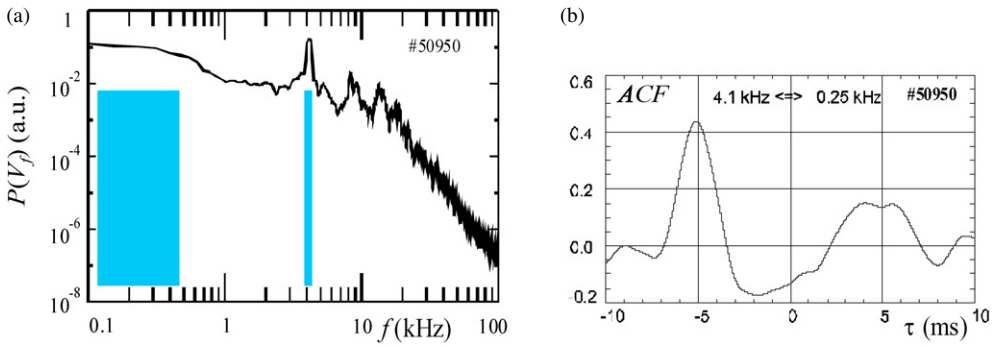

Figure 6. (*a*) Auto-power spectrum of the floating potential fluctuations in H-1 at $\rho = 0.5$ in L-mode at $B = 0.05$ T. Grey boxes indicate frequency bands used for the ACF analysis. (*b*) ACF between $f = 4.1$ kHz and $f = 0.25$ kHz bands (0.4 kHz bandwidths). Negative τ corresponds to the $f = 0.25$ kHz band leading in phase.

The energy flow direction is determined from the sign of the time lag τ at the maximum of the ACF. For example, if $x_1(t)$ and $x_2(t)$ correspond to the higher- and lower-frequency bands, $f_1 = 4.1$ kHz and $f_2 = 0.25$ kHz correspondingly, and if the ACF(τ) had a maximum at negative τ, it would mean that the amplitude of the higher-frequency-band lags with respect to the lower-frequency-band. This might be interpreted such that the high frequency band receives its energy from the low frequency band.

Figure 6(*a*) shows the spectrum of figure 4(*a*) in logarithmic scale along with the frequency bands selected for the analysis of the ACF. The ACF is shown in figure 6(*b*). The maximum of the ACF is about 0.45 and it is observed at the time lag of about $\tau = -5$ ms. This seemingly long time lag is close to one period of the low-frequency oscillations at 0.25 kHz chosen for the ACF analysis. This result may be suggestive of the coherent transfer of spectral energy from the $m = 0$ zero-frequency potential structure to the $m = 1$ coherent mode.

It is difficult to quantitatively characterize this energy transfer and to compare the efficiency of this transfer with the energy exchange between coherent structures (including the $m = 1$ mode) and the 'unstable' higher-frequency range reported in [14]. At this stage we may only conclude that there is strong coherent spectral coupling between mean zonal flow ($m = 0$, $f \approx 0$), coherent $m = 1$, $n = 1(2)$, $f = 4.1$ kHz mode (figure 6) and fluctuations in the higher-frequency range [14]. The analysis of spectral coupling between these three ranges will be presented elsewhere.

3. Geodesic curvature in the H-1 heliac

The evolution of the fluctuation spectra during the B-scan leading to the L–H transition in the H-1 heliac described above illustrates development of the GAM-like zonal flows. Similar $m = 0$ potential structures observed in other experiments are often interpreted as GAMs. Since most of the theoretical predictions and observations have been done for a tokamak geometry it is useful to evaluate if the geodesic effect is sufficiently strong in the magnetic configuration of the H-1 heliac.

According to the linear theory of the geodesic acoustic oscillation [12], a drive for the geodesic effect is proportional to $E \times B \cdot \nabla B^2/B^4$. Poloidal variation of B in toroidal devices is associated with the geodesic curvature, that is, the surface component of the magnetic field line curvature [12]. A parameter which we use here to characterize the geodesic curvature

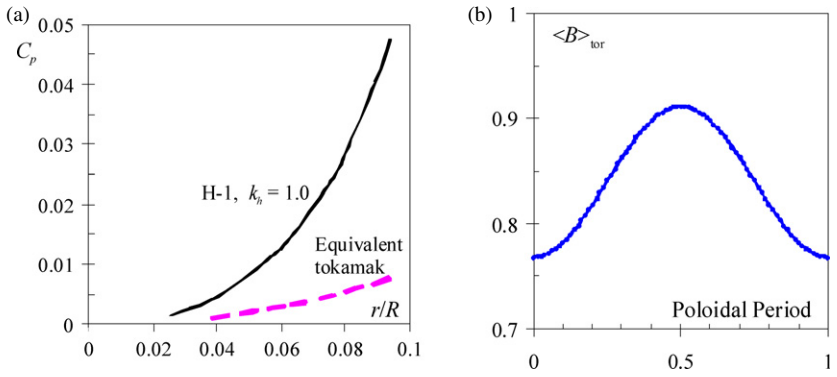

Figure 7. (*a*) Radial profiles of the poloidal viscous damping rate coefficient, $C_{\rm p}$, computed for the $\kappa_{\rm H} = 1$ configuration of the H-1 heliac (——) and for equivalent tokamak (- - - -). (*b*) Poloidal variation of the toroidally averaged magnetic field in the $\kappa_{\rm H} = 1$ configuration of the H-1 heliac.

is also a measure of the poloidal viscosity. We evaluate the poloidal viscous damping rate coefficient,$C_{\rm p} = \langle (e_p \cdot B/B)^2 \rangle$, derived in [28], which can be calculated from the variation of the magnetic field strength, B, in the poloidal direction in the Hamada coordinates. Here, B is the magnetic field vector, e_p is the poloidal base vector in the Hamada coordinates and brackets indicate the flux surface average. Larger $C_{\rm p}$ corresponds to larger geodesic curvature effect.

Computations of magnetic configurations of the H-1 heliac are based on the following steps: (1) magnetic field line tracing which utilizes a single filament model; (2) zero-pressure (zero-beta) equilibrium calculations using the VMEC-2000 code [29]; (3) transformation from VMEC coordinates to the Boozer coordinates [30] and finally, (4) transformation back to the Hamada coordinates. We will focus on the magnetic configuration, characterized by very low magnetic shear and relatively high rotational transform, $\iota = 1/q \approx 1.45$, which we will refer to as the $\kappa_{\rm H} = 1$ configuration. Here, $\kappa_{\rm H}$ denotes the ratio of the helical winding current to the current in the poloidal field coil. The poloidal cross section of the flux surfaces and the rotational transform profile for this configuration can be found in [31]. All experimental results presented in this paper have been studied in this magnetic configuration.

Figure 7(*a*) shows the radial profile of $C_{\rm p}$ for two cases, the H-1 $\kappa_{\rm H} = 1$ configuration, and the tokamak-like configuration. In the latter case of an equivalent tokamak, only contributions from axisymmetric components of the magnetic field spectrum in the Hamada coordinates are taken into account. The horizontal axis represents the geometrical inverse aspect ratio, r/R. It is obvious that $C_{\rm p}$ for the H-1 heliac is significantly larger than that in the equivalent tokamak. This difference arises from the variation in B due to higher poloidal mode numbers. Since poloidal mode numbers contribute to $C_{\rm p}$ in a square manner, the magnetic field components with higher poloidal mode numbers substantially increase $C_{\rm p}$ even if their amplitudes are relatively small.

The dominant mode of the pressure sideband of the geodesic acoustic oscillation predicted for a tokamak geometry appears to be the $m = 1$ mode [12]. We have tested if the presence of the higher poloidal numbers in the magnetic field spectrum of H-1 modifies toroidally averaged poloidal variation of B compared with an equivalent tokamak, since this can modify the principle mode number of the geodesic oscillations. The toroidally-averaged poloidal variation of B at the normalized radius of $\rho = r/\langle a \rangle \approx 0.5$ (inverse aspect ratio of $r/R \approx 0.085$) is shown in figure 7(*b*) for the case of $\kappa_{\rm H} = 1$. It is seen that the poloidal variation of B is

governed by the poloidal mode number of 1 (that is, $\cos\theta$ variation, where θ denotes the poloidal angle) as in a tokamak.

The above analysis suggests that a strong variation of a toroidal magnetic field on the flux surface in H-1 should have an even stronger effect on the compressibility of the $E \times B$ flow than in an equivalent tokamak (zonal flow faster on the outboard side of the torus) and thus may lead to geodesic transfer. Poloidal variation of a toroidally-averaged magnetic field is similar to the tokamak case, such that the poloidal mode number of $m = 1$ in the H-1 heliac should remain the same as in a tokamak.

4. Discussion

Several results described in sections 2 and 3 suggest that there may be a connection between the development of mean zonal flow (and mean E_r) and generation of coherent spectral features. Note that in this paper we do not clearly distinguish between mean zonal flows and mean local E_r generated via turbulence-independent mechanisms (e.g. neoclassical transport). This is an important issue and it will be addressed in a separate publication. In this paper the focus is on the link between mean (time-average) E_r and coherent modes in the GAM range. Observations which support the idea of such a connection are

(1) the correlation between the spectral energy contained in coherent modes and mean E_r shown in figure 3(*b*);
(2) the disappearance of all coherent modes during the L–H transition coincides with the proportional increase in the energy of the mean $E \times B$ flow as demonstrated in [17];
(3) the coherent spectral coupling between the nearly-zero-frequency band ($f = 0.25 \pm \Delta f$ kHz) and the $m = 1, n = 1(2)$ mode at $f = 4.1$ kHz of figure 6;
(4) the geodesic curvature in H-1 proportional to $C_\mathrm{p} = \langle (e_p \cdot B/B)^2 \rangle$ is larger than in an equivalent tokamak and thus generates substantial compressibility in the poloidal flow velocity in the poloidal plasma cross-section, $\nabla \cdot V \neq 0$. This mechanism may allow mean zonal flow to be coupled to the geodesic acoustic oscillation.
(5) reasonable agreement between frequencies of coherent modes and the frequency of the geodesic acoustic oscillation.

The frequency of GAM in H-1 can be by a factor of two to three higher than that in a tokamak (equation (1)), due to the shorter parallel connection length in H-1, $L_\parallel \approx 0.3$–0.4 m versus $L_\parallel = qR \approx 0.69$ m in an equivalent tokamak (in a real tokamak this should be even longer since $q > 1$). An estimate of the geodesic acoustic frequency in the H-1 plasma gives $f_\mathrm{GAM} = c_\mathrm{s}/L_\parallel \approx 4$–$5$ kHz.

Recently a linear theory of the GAM has been extended to stellarators [32]. By using a drift kinetic equation, a generalized dispersion relation of GAM has been obtained. The oscillation frequency is expressed in terms of sums of Fourier components of the magnetic field. We estimate the frequency of GAM in H-1 using the dispersion relation, equation (33) of [32], by retaining the ten most essential harmonics of the magnetic field spectrum B_mn in H-1. At the plasma mid-radius for $T_\mathrm{e} = 8$ eV and $T_\mathrm{i} = 30$ eV the GAM frequency appears to be $f_\mathrm{GAM} = 4.2$ kHz, which is close to the above elementary estimate and close to the observed frequency $f = 6.1$ kHz of the $m = 0$ mode in the spectrum of the floating potential of figure 4(*g*).

One should keep in mind that spectra of figure 4 are measured in the lab frame such that the frequencies of the spectral components are Doppler-shifted due to the plasma drifts

$$\omega_\mathrm{lab} = k_\theta V_\mathrm{D} + \omega_\mathrm{plasma}. \tag{4}$$

This Doppler shift does not affect the $m = 0$ modes but does change the frequencies of other spectral components. Figure 4(c) shows two spectral features having $m = 1$ at $f \approx 1$ kHz and $m = -1$ at $f \approx 8$ kHz. Equation (4) can be rewritten for these two modes by substituting k_θ with $m/r = \pm 1/r$ as $\omega_{\rm lab}^{m=1} = (1/r)V_{\rm D} + \omega_{\rm plasma}^{m=1}$, and $\omega_{\rm lab}^{m=-1} = (-1/r)V_{\rm D} + \omega_{\rm plasma}^{m=-1}$. Since in the plasma frame $\omega_{\rm plasma}^{m=1} = \omega_{\rm plasma}^{m=-1}$, by adding the above equations one can obtain $\omega_{\rm plasma}^{m=1} = 1/2(\omega_{\rm lab}^{m=1} + \omega_{\rm lab}^{m=-1})$. This gives for the $m = \pm 1$ mode in the spectrum of figure 4(c) frequency in the plasma frame of $f \approx 4.5$ kHz. This is very close to the frequency $f \approx 4.1$ kHz of the $m = 1$ mode in figure 4(a) measured at lower $E \times B$ drift (lower E_r) and also very close to the above estimates of the GAM frequency.

Several observations reported here cannot be easily explained by simple linear theory of GAM [12, 32].

GAM is a linear oscillation which should be observed even at modest $\nabla \cdot V \neq 0$. In our experiment, the $m = 0$, $n = 0$, $f \approx f_{\rm GAM}$ potential structure is observed only at sufficiently high radial electric fields, following the development of other $n \neq 0$ coherent modes. It is possible that such a threshold in geodesic 'drive' (proportional to $E \times B \cdot \nabla B^2/B^4$) observed in our experiments has to do with the existence of damping in the process of the excitation of the GAM-like feature. Collisional damping of GAM due to the ion–ion collisions should be small in our experiments. Collisionless damping cannot be essential in the mechanism of the GAM excitation either, since zonal flows and GAM are modes of minimal Landau damping [2].

In our experiments, however, the development of the GAM-like feature is always preceded by the onset of other coherent modes ($n \neq 0$, $m = 1, 2, \ldots$). These modes can be Landau damped by ions if their phase velocity along B becomes close to the ion thermal velocity, $V_{\rm ti}$. For the $m = 1$ mode having $k_\parallel \approx 2\,{\rm m}^{-1}$ at $f \approx 4$ kHz (figure 4(a)) parallel phase velocity is of the order of $V_{\parallel ph} = \omega/k_\parallel \approx 1.2 \cdot 10^4\,{\rm m\,s}^{-1}$, which is quite close to $V_{\rm ti} \approx 1 \cdot 10^4\,{\rm m\,s}^{-1}$. Thus, Landau damping on ions of the finite-n coherent modes may be responsible for the observed 'threshold' generation of GAM in H-1.

The theory of GAM predicts generation of the following GAM-related oscillations: the $m = 1$, $n = 0$ pressure sideband oscillation observed in the density and the $m = 0$, $n = 0$ coherent oscillation in the electrostatic potential which develop simultaneously [2]. In our experiments we observe the development of the $m = 1$, $n = 1$ (2?) mode in both density and potential (figures 4(a) and (b)), followed by the development of the $m = 2$, $n = 2$ (3?) mode (figures 4(c) and (d)) and then the onset of the $m = 0$, $n = 0$ GAM-like spectral feature in the potential (figure 4(e)–(h)).

The onset of the $m = 0$, $n = 0$ GAM-like structure is observed close to the threshold for the L–H transition in H-1. When the magnetic field is increased above some critical value, the fluctuation level is greatly reduced, while the mean E_r is further increased securing the confinement transition to H-mode. In the case of the B-scan illustrated in figures 3 and 4 this critical magnetic field is $B \approx 0.063$ T. As has been previously reported [24], the L–H transition threshold in the shear of E_r agrees reasonably well with an estimate of the E_r - shear decorrelation of the low-m coherent modes. Namely, the E_r shear produces a shearing decorrelation rate [27] of

$$\tau_{\rm s}^{-1} = \left[\frac{k_{\rm pol}\Delta r_{\rm m}}{B_{\rm T}}\frac{{\rm d}E}{{\rm d}r}\right], \tag{5}$$

where $\Delta r_{\rm m}$ is the radial mode width (0.04–0.05 m in our case) and $k_{\rm pol}$ is the poloidal wave number ($k_{\rm pol} \sim 12\,{\rm m}^{-1}$, for the $m = 1$ mode). In the conditions described in this paper $(1/\tau_{\rm s}) \approx 1 \times 10^5\,[{\rm litres}]\,{\rm s}^{-1}$, which is larger than the turbulence decorrelation rate $\tau_{\rm D}^{-1} = D_{\rm an}/\Delta r_{\rm m}^2 \sim 2.5 \times 10^4\,{\rm s}^{-1}$, where $D_{\rm an} \approx 40\,{\rm m}^2\,{\rm s}^{-1}$ is the anomalous diffusion

coefficient, estimated by comparing particle fluxes in low and high modes [11]. Thus, our results agree with the E_r shear suppression model when the condition $1/\tau_s \gg 1/\tau_D$ is satisfied just before the transition to H-mode.

The results presented here point to the following scenario of the L–H transitions in H-1. As the mean zonal flow develops in the plasma, coherent oscillation having $m = 1$ at the GAM frequency develops. As the spectral energy delivered from the broadband turbulence to the mean zonal flow is further increased, both $\langle E_r \rangle$ and the energy of coherent low-m modes are increased. When $\langle E_r \rangle$ and its shear reach the E_r-shear decorrelation threshold, the $m = 1$ mode can no longer exist, thus closing the energy escape route for the mean zonal flow. This leads to a further jump in $\langle E_r \rangle$ and to the suppression of other low-m modes ($m = 1, 2, \ldots$). It is possible that the shear decorrelation criterion needs to be satisfied only for the $m = 1$ mode and this will lead to the suppression of all other coherent modes.

Such a scenario also agrees with our result in [17] where it has been shown that the reduction in the radial integral of the energy contained in turbulence (mostly the energy of coherent modes) during L–H transitions to within 20% agrees with the increase in the energy of the $E \times B$ flow. Thus the energy accumulated in the coherent modes goes back to the mean zonal flow.

Acknowledgments

The authors thank Horst Punzmann for useful discussions. Part of this work has been done during MY's visit to the Plasma Research Laboratory, Australian National University (PRL, ANU) as the Visiting Academic, which is supported by the Ministry of Education, Culture, Sports, Science and Technology of Japan. The sincere hospitality of the colleagues in PRL, ANU is highly appreciated.

References

[1] Hasegawa A, Maclennan C G and Kodama Y 1979 *Phys. Fluids* **22** 2122
[2] Diamond P H, Itoh S-I, Itoh K and Hahm T S 2005 *Plasma Phys. Control. Fusion* **47** R35
[3] Shats M G and Solomon W M 2002 *Phys. Rev. Lett.* **88** 045001
[4] Jakubowski M, Fonck R J, Fenzi C and McKee G R 2002 *Phys. Rev. Lett.* **89** 265003
[5] McKee G R, Fonck R J, Jakubowski M, Burrell K H, Hallatschek K, Moyer R A, Nevins W, Rudakov D L and Xu X 2003 *Plasma Phys. Control. Fusion* **45** A477
[6] Coda S, Porkolab M and Burrel K M 2001 *Phys. Rev. Lett.* **86** 4835
[7] Fujisawa A *et al* 2004 *Phys. Rev. Lett.* **93** 165002
[8] Hamada Y *et al* 2005 *Nucl. Fusion* **45** 81
[9] Conway G D 2005 *Plasma Phys. Control. Fusion* **47** 1165
[10] Shats M G, Solomon W M and Xia H 2003 *Phys. Rev. Lett.* **90** 125002
[11] Punzmann H and Shats M G 2004 *Phys. Rev. Lett.* **93** 125003
[12] Winsor N, Johnson J L and Dawson J M 1968 *Phys. Fluids* **11** 2448
[13] Xia H and Shats M G 2003 *Phys. Rev. Lett.* **91** 155001
[14] Xia H and Shats M G 2004 *Phys. Plasmas* **11** 561
[15] Crossley F J *et al* 1992 *Plasma Phys. Control. Fusion* **34** 235
[16] Kraichnan R H 1967 *Phys. Fluids* **10** 1417
[17] Shats M G, Xia H and Punzmann H 2005 *Phys. Rev.* E **71** 046409
[18] Scott B 2003 *Phys. Lett.* A **320** 53
[19] Scott B D 2005 *New J. Phys.* **7** 92
[20] Itoh K, Hallatschek K and Itoh S-I 2005 *Plasma Phys. Control. Fusion* **47** 451
[21] Hamberger S M *et al* 1990 *Fusion Technol.* **17** 123
[22] Shats M G *et al* 1996 *Phys. Rev. Lett.* **77** 4190

[23] Shats M G *et al* 1998 *Phys. Plasmas* **5** 2390
[24] Shats M G 1999 *Plasma Phys. Control. Fusion* **41** 1357
[25] Crossley F J *et al* 1992 *Plasma Phys. Control. Fusion* **34** 235
[26] Horton W and Hasegawa A 1994 *Chaos* **4** 227
[27] Biglari H, Diamond P H and Terry P W 1990 *Phys. Fluids* B **2** 1
[28] Wobig H *et al* 1995 *Plasma Phys. Control. Fusion* **37** 893
[29] Hirshman S P and Whiston J C 1983 *Phys. Fluids* **26** 3553
[30] Boozer A H 1980 *Phys. Fluids* **23** 904
[31] Shats M G *et al* 1994 *Nucl. Fusion* **34** 1653
[32] Watari T *et al* 2005 *Phys. Plasmas* **12** 062304